EXPERIMENTAL EVALUATION OF PHOTO-ACTIVATED CROSS-LINKING EFFECTS ON MECHANICAL PROPERTIES OF ARTERIES POST-ANGIOPLASTY

by

Farshad Mogharrabi

A thesis submitted to the faculty of
The University of Utah
in partial fulfillment of the requirements for the degree of

Master of Science

Department of Mechanical Engineering

The University of Utah

February 2021

The University of Utah Graduate School

STATEMENT OF THESIS APPROVAL

The thesis of **Farshad Mogharrabi**

has been approved by the following supervisory committee members:

Kenneth L. Monson	, Chair	**date approved** Date Approved
Brittany Coats	, Member	**date approved** Date Approved
Lucas H. Timmins	, Member	**date approved** Date Approved

and by **Bruce K. Gale** , Chair/Dean of

the Department/College/School of **Mechanical Engineering**

and by David B. Kieda, Dean of The Graduate School.

ABSTRACT

Percutaneous transluminal angioplasty (PTA) is a medical procedure performed on patients with severe atherosclerosis to open up stenosed blood vessels by inflating a balloon at the narrowing location. In many cases of PTA, restenosis occurs post-surgery due either to elastic behavior of the artery, also known as elastic recoil in medical literature, or to plaque reformation within the lumen. For that reason, stents are commonly deployed to keep the arterial lumen open. Stent deployment causes problems in some cases; for example, the presence of stents in arteries with frequent movements and large deformations can cause ruptures in the arterial wall.

Recent studies on 1,8-Naphthalimide organic compounds have shown that when these compounds are activated using a specific wavelength of light, it causes cross-linking between the components of the extracellular matrix. This observation has led to studies with the goal of developing a method to utilize this process to replace stents for cases with limiting conditions for stent deployment. Therefore, Natural Vascular Scaffolding (NVS) has been drawing experts' attention in the field.

In this study we focused on measuring and quantifying the effects of NVS on the mechanical properties of healthy arteries undergoing PTA under various loading conditions. The results of the experiments show that NVS treatment results in a significant increase in working diameter, in the absence of changes to vessel stiffness. These results suggest that NVS may be effective alternative to mechanical stents.

Note that most of this work as been published elsewhere as Mogharrabi, F., J. Kuhlenhoelter, B. Anderson, K. Kauser and K. Monson (2019). Effect of Photoactivated Cross-Linking Compound on Mechanical Properties of Porcine Carotid Arteries Post-Angioplasty. ASME 2019 International Mechanical Engineering Congress and Exposition, American Society of Mechanical Engineers Digital Collection.

To Yuan-Cheng Fung, father of biomechanics, may he rest in peace.

(The journey to get to your goal is not easy, so take it easy on yourself)

TABLE OF CONTENTS

LIST OF TABLES

Tables

LIST OF FIGURES

Figures

ACKNOWLEDGMENTS

In writing this thesis, not only did I learn what is meant to learn as a scholar, but also I learned life-lessons that will forever stay with me. The lessons that one cannot simply learn from a book. I want to thank my academic advisor, Dr. Ken Monson, and my colleagues at the Head Injury and Vessel Biomechanics Laboratory at the University of Utah, since without their help and support, I would not be where I am today.

CHAPTER 1

INTRODUCTION

1.1 Significance of Cardiovascular Disease

Cardiovascular disease is the leading cause of death in the modern world, with 735,000 United States (U.S.) citizens having a heart attack annually [1]. Severe atherosclerosis cases may include complete blockage of blood flow, plaque rupture, and embolism, leading to damage of downstream organs and tissues. Peripheral artery disease (PAD) occurs when atherosclerosis develops in one of the vessels terminating in the limbs. About 8 million Americans were diagnosed with PAD in 2012 [2]. The disease affects both genders equally but becomes more prevalent with age, to the extent that up to 20 percent of the population of the U.S. over 65 years of age are affected by it [2]. Also, because causes of this health disorder, including high blood pressure, diabetes, and high cholesterol, are becoming more prevalent, the development of effective treatments is critical.

1.2 Transluminal Angioplasty

A common treatment for PAD is percutaneous transluminal angioplasty (PTA). This procedure consists of pressurizing a balloon inside the stenosed artery with the goal of permanently dilating the lumen to overcome the lack of blood flow. The mechanisms

by which the procedure works are not fully understood [3]. Although early views suggested compression and deformation of the plaque, recent work indicates that the mechanisms are more complex, implicating overstretch of the vessel wall along with some deformation or fracture of the plaque.

In 29.3 percent of cases, PTA is not successful on PAD [4], and restenosis occurs, which is assumed to be due either to the natural elastic recoil of the artery to its native configuration or to a response to the damage caused to healthy regions of artery around the plaque. To avoid restenosis, a stent is often deployed to keep the lumen open. Stents are cylindrical mechanical structures, generally made from biocompatible metals or plastics, that are placed at the plaque location to keep the blood vessel dilated.

1.3 Natural Vascular Scaffolding

Stent placement can be problematic at locations where blood vessels experience repeated large deformations, such as near limb joints, since the rigid device may be loosened or further damage the blood vessel. Natural Vascular Scaffolding (NVS), a novel treatment exposing vessels to a photoactivated cross-linking compound during balloon angioplasty, is currently under study as a potential alternative to stenting in such regions. Previous experiments showed that NVS-treated vessels maintained a larger diameter post-angioplasty than controls exposed to angioplasty alone [5]. While these results are promising, the testing in this study was not thorough enough to conclude the effectiveness of NVS under in vivo circumstances. The measures reported in this study, like *cross-sectional compliance* and *distensibility coefficient,* are not commonly used when reporting mechanical properties of soft tissue. Also, there were some inaccuracies

in the design of the experiments compared to an actual in vivo treatment. For example, during the tests, the in vivo axial stretch conditions were not simulated, and the experiments were performed under a single circumferential stretch. Also, the samples were soaked in NVS compared to the more practical approach of covering up the inner lining of the artery lumen with the drug for treatment.

1.4 Objective

In the current study, we characterized changes in the multiaxial mechanical behavior of NVS-treated porcine carotid arteries. Both NVS-treated and control samples were tested for comparison. The influence of treatment on the behavior of samples was evaluated under various combinations of circumferential and axial stretch to better understand the influence of these conditions. Loading combinations were chosen that are similar to in vivo conditions.

CHAPTER 2

MATERIALS AND METHODS

2.1 Sample Preparation

Fresh carotid arteries from 6 to 9-month-old pigs were acquired from Animal Technologies Inc. (Tyler, TX) and shipped to our laboratory overnight in coolers containing ice. All treatments and testing procedures were performed within 48 hours of animal death to limit the influence of soft tissue degradation that leads to changes in tissue response [6]. Samples were kept in vials filled with phosphate-buffered saline (PBS) refrigerated at 4 degrees Celsius before testing and were tested at room temperature.

We examined each carotid artery visually for abnormalities and defects that might have been inherited by the animal or imposed on the tissue during dissection. Defective specimens were discarded. From the selected samples, we extracted the region with the least branching and diameter variation over their length by visual inspection under a magnifying lens.

At this stage, each blood vessel was cut into two samples, one for treatment with NVS and one to serve as a control. We split the samples such that each of the two samples created had close geometrical characteristics in order to keep the results relatively comparable. Despite the similar sizing of the sample pairs, inevitably,

variations over the sample diameter and wall thickness existed over the length of each specimen. To account for this variation, for all the cases that allowed, we performed cross-sectional measurements on both ends. Hence, we took the average of the measured values from both ends as the representative dimensions of the tested sample. For the samples that were too small to cut two rings from, which had uniform cross-sectional dimensions by visual inspection, only one ring was dissected and measured.

To measure the cross-sectional dimensions of samples, as mentioned above, we cut a thin ring from the ends of each blood vessel. The rings were cut perpendicular to the axis of the lumen using a surgical scalpel to minimize geometric disruption. The rings were laid on their flat side in a petri dish filled with room temperature PBS with a scale adjacent to them for image acquisition. Images were taken using a digital camera (Pixelink, PL-A641) attached to a stereo microscope (Zeiss, Stemi 2000-C) available at the Head Injury and Vessel Biomechanics laboratory. We used a custom MATLAB script (Appendix A) to calculate the dimensions from these images (Figure 2.1). In the script for cross-sectional calculations, we assigned a series of points to the outer and inner perimeters of the cross-sections imaged. These points were transformed into polygons to model the boundaries defining the arterial wall. The polygons are then assumed to be circles by averaging the defining points' distance to their centroid to calculate approximate inner and outer diameters. These values were used to calculate the average wall thickness. We initially calculated all the values above in pixels, and then using the scale in the images, we converted them to SI units.

2.2 Experimental Groups

As specified earlier, each blood vessel was cut into two segments, one for treatment with NVS and one to serve as a control. We refer to these two specimens as a pair. A total of 28 sample pairs were tested successfully.

To identify the circumstances under which NVS treatment has a significant effect on the artery, we defined four different loading combinations to study the influence of various loads and to mimic in vivo PTA loadings at the time of treatment (Table 2.1). Sample groups were defined as the binary combination of two variables: (1) being "ballooned" or not and (2) being "axially stretched" or not. Although samples that were not axially stretched do not accurately resemble in vivo conditions, they were included to provide additional insight about the working mechanism of NVS.

In Groups 1 and 2, samples were axially stretched to approximately 1.6 times their unloaded length at the time of NVS treatment, the typical in vivo axial stretch of porcine carotids [7]. This assumption was confirmed by our experiments later, which showed that the average in vivo axial stretch for these vessels was about 1.73 (see Section 3). In Groups 2 and 4, NVS treatment was performed while blood vessels were circumferentially stretched to a stretch ratio of about 1.3, using an angioplasty balloon on the optical catheter used for NVS treatment, to be representative of procedural PTA circumferential stretch levels [8]. The angioplasty balloon length was chosen to be longer than the region of the artery that we wanted to test so that it would stretch the testing region almost uniformly without leaving end effects.

Vessels were treated with NVS by filling the lumen with the NVS compound (dimeric substituted-1,8-naphthalimide)[5] for 5 minutes to allow diffusion into the

vessel wall. A customized optical catheter with a balloon at its tip was then guided into the lumen to shine a 457 nm laser, for 1 minute, onto the treatment region to activate the NVS and induce cross-linking. The laser-induced cross-linking was performed while each vessel was maintained at the mechanical conditions defined for its assigned testing group. For the samples that were part of the ballooned group (Groups 2 and 4), this integrated balloon was used to produce the circumferential stretch during the treatment. Following treatment, evaluation of mechanical properties was conducted using the same protocol for all of the samples, as described in the following sections.

2.3 Testing Apparatus

To characterize any changes in the mechanical properties of the samples, biaxial mechanical tests were conducted using a custom-built pressure myograph device (Figure 2.2) used in previous studies [9]. The myograph device consists of three major components. The first component controls the applied displacements (along the first axis). Another device controls the flow of saline to and from the specimen. Therefore, the pressure is controlled by this unit (along the second axis, i.e., the circumference). The third major component is the computer with its accompanying test control and data acquisition (DAQ) system with a visual interface (VI; LabVIEW; National Instruments) to control and synchronize the motors and to acquire sensor and image data from the experiments (Figure 2.3).

The main testing platform consists of a stepper motor, an encoder, and two moving platforms (Figure 2.2, items 1 to 4). The motor drives the two screw-driven platforms to move simultaneously in opposing directions. This equally-paced diverging

or converging motion allows for the midplane between the platforms to be stationary, allowing for convenient visual data acquisition from the specimen located close to this plane. The encoder captures the angular motion of the actuator and sends it to the VI unit for decoding and compiling into displacement values.

Axial force measurement is done by the first unit as well. Forces were measured using a 1.1-kg capacity load cell (MDB-2.5, Transducer Techniques). The load cell was mounted to a micro-positioner attached to the top moving platform (Figure 2.2, items 5 and 6). The micro-positioner was adjusted to minimize non-axial forces due to axis offset in upper and lower mounts. Transducer data were collected at a rate of 100 Hz using a NI DAQ unit(SCXI-1520, National Instruments).

The pressure control unit manipulates the circumferential loading by pressurizing the specimen. This unit consists of a linear actuator connected to a syringe that feeds a tube to the specimen. The tube conducts saline through manual control valves, past pressure sensors, and into specimen-mounting blocks (Figure 2.2, items 7 to 13). The mounting blocks have free-rotating male Luer lock pieces to adjust rotation in the upper and lower ends of the specimen, avoiding unwanted torsional stresses during testing. The pressure was measured using two transducers (Honeywell, MicroSwitch 26PCDFM6G) positioned upstream and downstream from the sample for averaging (Figure 2.3).

The entire system is controlled using a VI programmed in NI LabView software. The VI receives pressure, displacement, and force values from the units and sends commands to the pressure and displacement actuators, controlling these values through a feedback loop (Figure 2.3, LabView VI block).

Deformation, including outer diameter and axial stretch, was captured and directly

sent to the VI using a digital camera (PL-A641, Pixelink) at 3 frames per second. To match the deformation from images with the other acquired sensory data, the deformation data points were up-sampled to match the frequency of the transducer data.

2.4 Testing Procedure

Vessels were mounted on standard 1/8 in (3.2 mm) barb fittings (MK-45552-04 Nylon female Luer x 1/8" wide-mouth hose barb fitting, Cole-Parmer). Two knots were tied around each end of the sample and barbs using 3-0 suture, and both ends of the vessel were adhered to the barbs using cyanoacrylate glue to ensure the connection would not leak saline during pressurizing.

To ensure optimum capturing of tissue deformation during testing, the camera was placed and calibrated such that it would always capture the center of the sample (Figure 2.4). The center of the sample remained within camera view throughout the test as the mounting plates move at the same speed.

The samples were then mounted on the channeled blocks on the myograph stage using Luer locks of the barb fittings. The blocks have holes machined into them to allow for fluid flow through the sample. PBS was used within the hydraulic circuit of the testing setup to both pressurize and hydrate the samples. A drop of saline was also periodically applied to the outside of the sample during testing.

During the first stage of the test, we determined the in vivo length of each sample. This is crucial because this value was then used as a reference to make comparisons meaningful. The in vivo length was identified as the point where axial force remained constant with alterations in pressure[10]. Starting from the resting length and for

increasing axial stretch values, we pressurized the samples for five cycles, between 6.7 kPa and 22 kPa. Multiple cycles were done to reduce the hysteresis effect. Usable axial force values were extracted over the last pressurization cycle. If the force and pressure showed reverse behavior, we could identify we had gone above the in vivo length, and at stretches below the in vivo length, both force and pressure increased or decreased simultaneously (Figure 2.5). For confirmation of accurate in vivo length, we would stretch the vessel 5% beyond the determined in vivo length to observe the reverse force-stretch behavior for every sample. On average, around ten iterations were enough to find in vivo length to within a 0.1 mm margin, which would lead to errors less than 1 percent of sample length for a 15 mm sample.

The next step was to find the zero-load length (ZLL) of the sample. This was to find the length at which the sample would experience no axial force when not pressurized, corresponding to the zero-load configuration. For this test, we depressurized the sample and then stretched it from slightly below resting length (from an initially buckled configuration) up to 1.10x the in vivo length. We did this for five cycles to achieve steady-state and then used the last cycle to measure the ZLL.

The samples were then biaxially loaded in six different configurations to establish their response: circumferentially (up to 22.5 kPa) while held at 1.00x, 1.05x, and 1.10x times in vivo axial stretch and axially (up to 1.10 times in vivo stretch) while held at 9.2, 15.8, and 22.5 kPa luminal pressure. All loading was done quasi-statically. This biaxial sequence was performed both before and after the NVS treatment procedure described above (Section 2.2) to determine the effect of the treatment. Control samples were exposed to the same six configurations of biaxial tests only without any NVS treatment .

For the purposes of this study, only testing configurations most similar to the in vivo configuration (1.00x axial in vivo stretch and 15.8 kPa luminal pressure) were evaluated.

2.5 Calculations and Parameters

Cauchy stress (T_i) and stretch (λ_i) in both the axial ($i = z$) and circumferential ($i = \theta$) directions were calculated using the collected experimental data along with equations (2.1) to (2.4), assuming the vessels were accurately represented as hollow cylindrical tubes.

$$\lambda_\theta = \frac{d_i + d_o}{D_i + D_o} \tag{2.1}$$

$$T_\theta = P \frac{d_i}{d_i - d_o} \tag{2.2}$$

$$\lambda_z = \frac{l}{L} \tag{2.3}$$

$$T_z = \frac{\lambda_z}{A}\left(F_z + \frac{\pi}{4} P d_i^2\right) \tag{2.4}$$

In these equations, d_i and d_o represent, respectively, the inner and outer diameter of the blood vessel at each data point over the test; D_i and D_o represent the unloaded values for inner and outer diameter; P is the luminal pressure; l and L are, respectively, the current and unloaded lengths of the sample along the tube axis; A is the cross-sectional area of the sample wall; and F_z is the axial load samples experienced over the test at each data point.

Required reference configuration parameters, such as vessel diameters, wall thickness, and cross-sectional area, were obtained through the measurement of scaled

images of cross-sections taken from the ends of the samples, as previously explained. The current configuration internal diameter was determined using these values and by assuming incompressibility.

In vivo stiffness was defined as the slope of the stress-stretch curve at in vivo stretch. Each stress-stretch curve was fit with an exponential function (Figure 2.6) to facilitate analysis. The fit optimization was done using the least squares method. The stiffness was calculated by finding the value of the derivative of the exponential fit function at the in vivo configuration (MATLAB code available under Appendix A).

Comparisons were made between the control and treated samples to determine the influence of NVS treatment. Using equations (2.5) and (2.6), we defined the *Change in In Vivo Circumferential Stretch* and the *Change in In Vivo Circumferential Stiffness* parameters for each sample pair to compare to the other pairs of the same group.

$$\Delta\lambda_{\theta_{IV}} = \left(\lambda_{\theta_{IV}}\right)_{NVS} - \left(\lambda_{\theta_{IV}}\right)_{Control} \tag{2.5}$$

$$\Delta\frac{dT}{d\lambda_\theta} = \left(\frac{dT}{d\lambda_\theta}\right)_{NVS} - \left(\frac{dT}{d\lambda_\theta}\right)_{Control} \tag{2.6}$$

Differences between both in vivo stretch and in vivo stiffness in each pair were calculated. Comparisons were based on the shift observed in the paired samples exponential fit function.

2.6 Statistical Analysis

To evaluate the significance of the calculated results, statistical analysis was performed as described in this section, and results with p-values less than 0.05 were taken

as significant. The two different parameters considered statistically were the change of in vivo circumferential stretch and the change in the circumferential stiffness. The data regarding the observed change for each of the groups is presented in the next chapter (Table 3.2).

One-sample t-tests were performed within each group to evaluate whether the treated samples differed from controls. This was done by calculating the mean ($\bar{x}$) and standard deviation (STD) of each group.Then the p-value associated with the calculated t-value (t) on a one-tailed t-distribution was obtained to evaluate changes. The equations (2.7) and (2.8) were used for this process.

$$S_{\bar{x}} = \frac{\mathrm{STD}}{\sqrt{n}} \tag{2.7}$$

$$t = \frac{\bar{x}-\mu}{S_{\bar{x}}} \tag{2.8}$$

Please note that here, μ, is the hypothesized value for the change, which was assumed to be zero. Therefore, if rejected by p-values lower than 0.05, we would consider the results to be significantly different from the hypothesized value. Results of this analysis are presented in the next chapter (Table 3.3).

To make comparisons between the groups, ANOVA analysis of variance was done on the same two parameters mentioned. Initially, homogeneity of variances in groups was evaluated using Levene's test. For values with homogeneous variances, simple one-way ANOVA was used, and for values that showed non-homogeneous variances, Welch's ANOVA was applied. Where these tests identified significant differences, post-hoc group-to-group comparisons were determined to be significant by

comparing p-values using the Bonferroni correction that considers the number of groups involved. No post-hoc tests were performed as they were not necessary.

Table 2.1 Loading conditions at the time of treatment for the different experimental groups. Axially stretched samples were stretched to 1.6 times their resting length. Ballooned samples were circumferentially stretched using a PTA balloon chosen according to the size of the vessel to reach about 30% circumferential stretch according to standard operating room procedures[7,8].

Testing Group	Ballooned	Axially stretched	Number of pairs
Group 1	No	Yes	6
Group 2	Yes	Yes	7
Group 3	No	No	7
Group 4	Yes	No	8

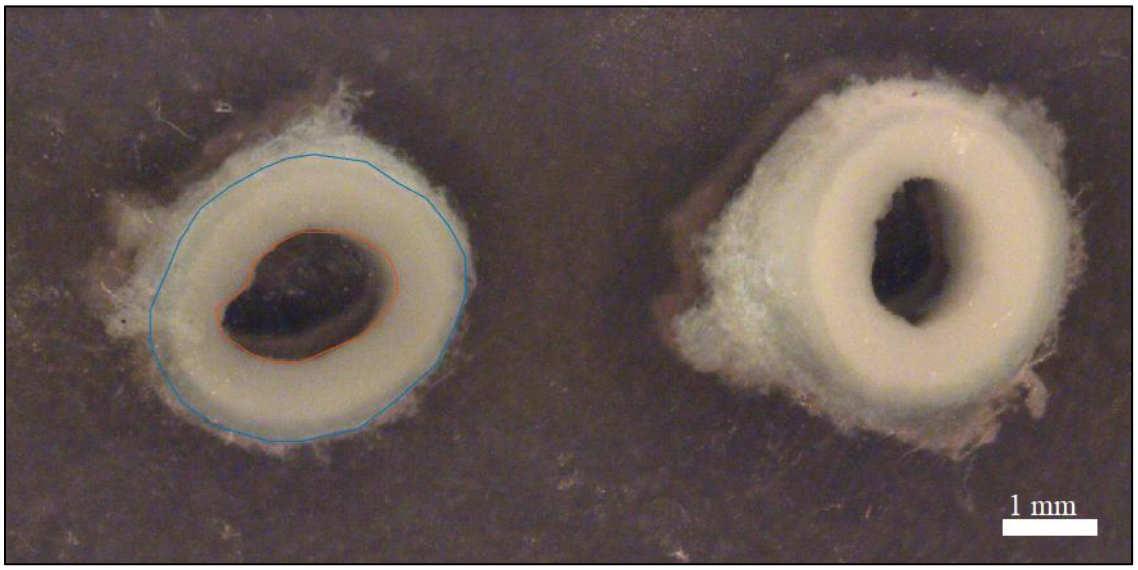

Figure 2.1. Rings of a carotid artery dissected from both ends of the sample to measure the cross-sectional dimensions. On the left, the ring has been marked by the custom code to evaluate the sample: The blue line shows the polygon fitted to the outer surface of the sample, and the red line defines the luminal boundary.

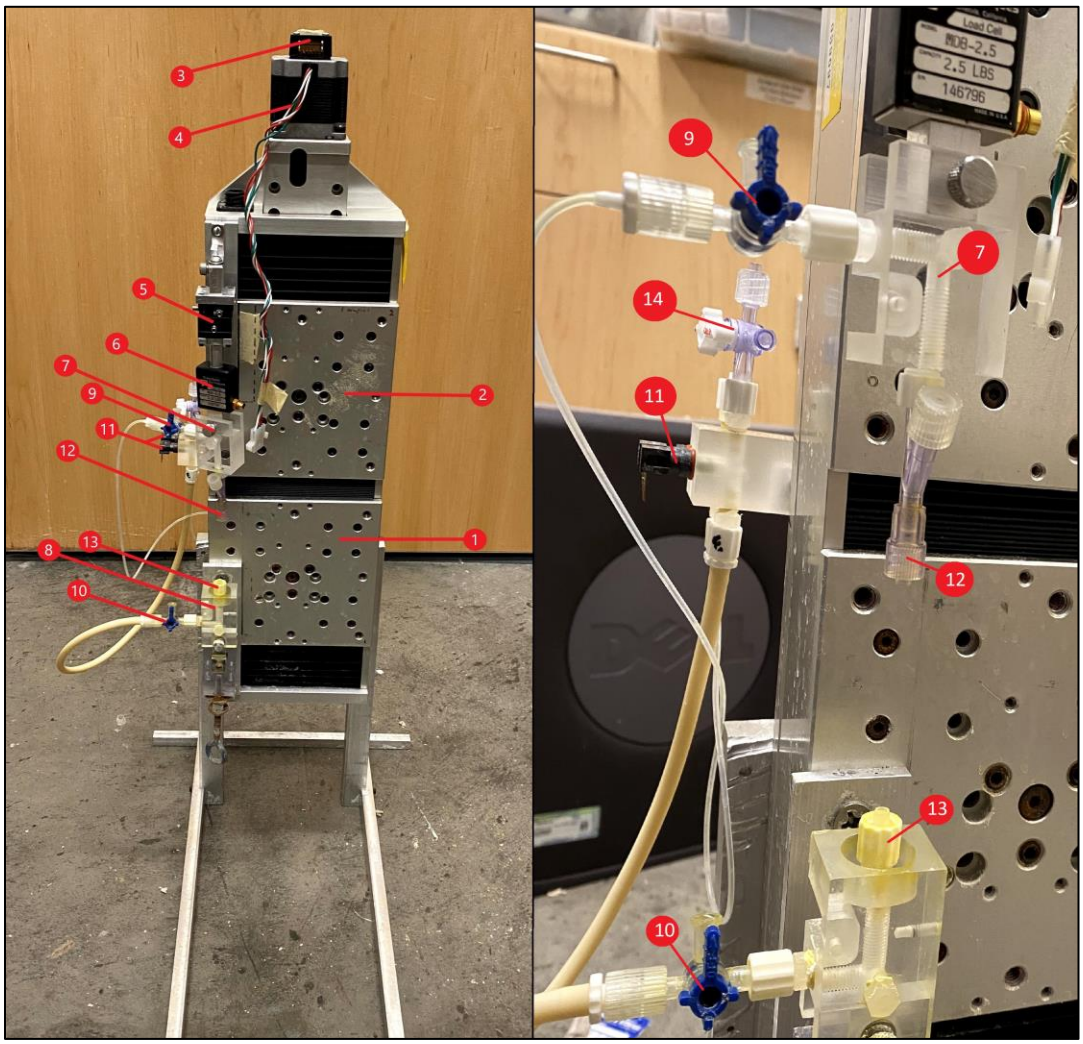

Figure 2.2. Custom-built myograph device for biaxial mechanical testing of blood vessels; Zoomed in view on the right; Significant parts of the device are: (1,2) lower and upper moving platforms with screw holes, (3) digital encoder to measure plate movement, (4) stepper motor to control plate movement, (5) micro-positioner, (6) load cell, (7,8) upper and lower mounting blocks with flow channels (9,10) upper and lower flow valves controlling the flow to the pressure transducers, (11) pressure transducers, and (12,13) upper and lower male Luer locks for sample attachment, (14) valve to atmospheric pressure.

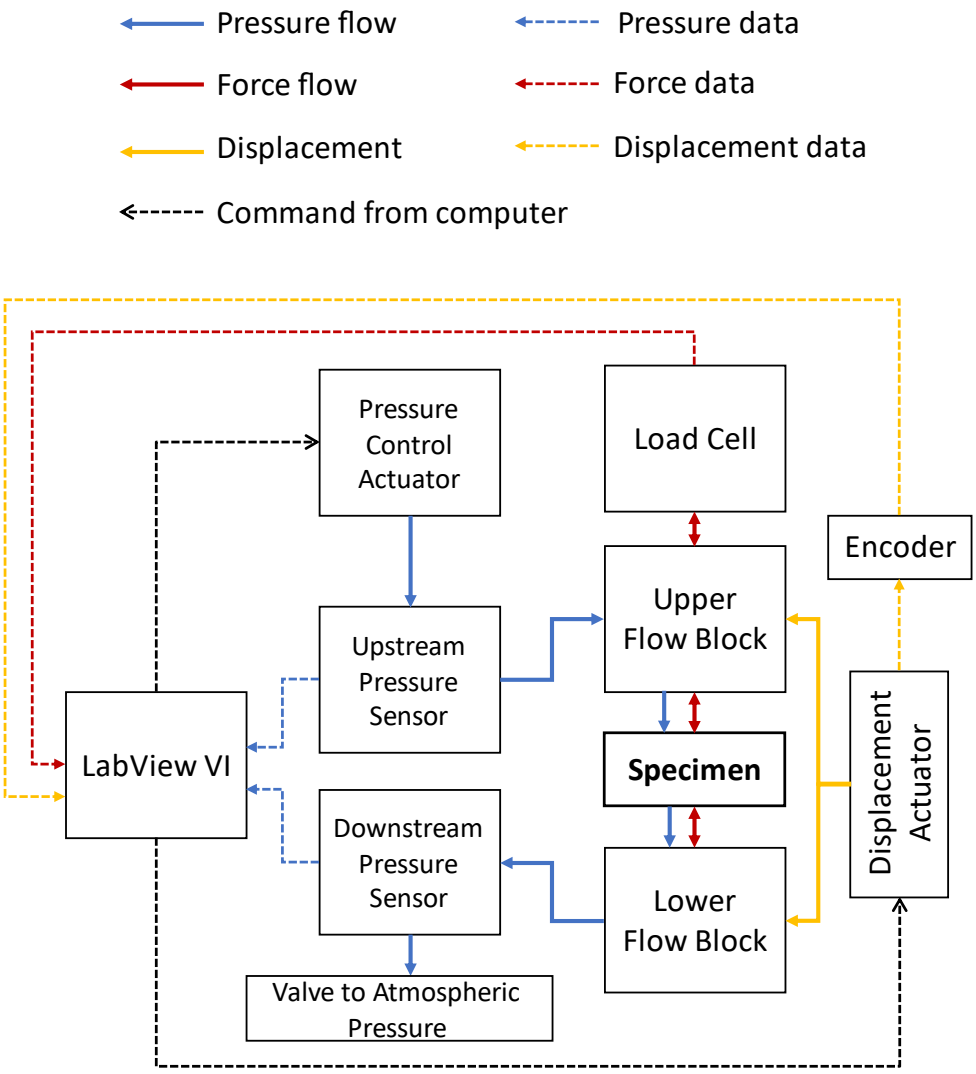

Figure 2.3. A schematic of the myograph device interactions and signals. Within the pressure control unit, the flow starts from the "Pressure Control Actuator" and is shown using blue arrows. The "LabView VI" block represents the computer and the DAQ unit together.

Figure 2.4. A sample image of the specimen during the testing. The middle part of the artery that remains stationary during axial stretching was recorded for each test.

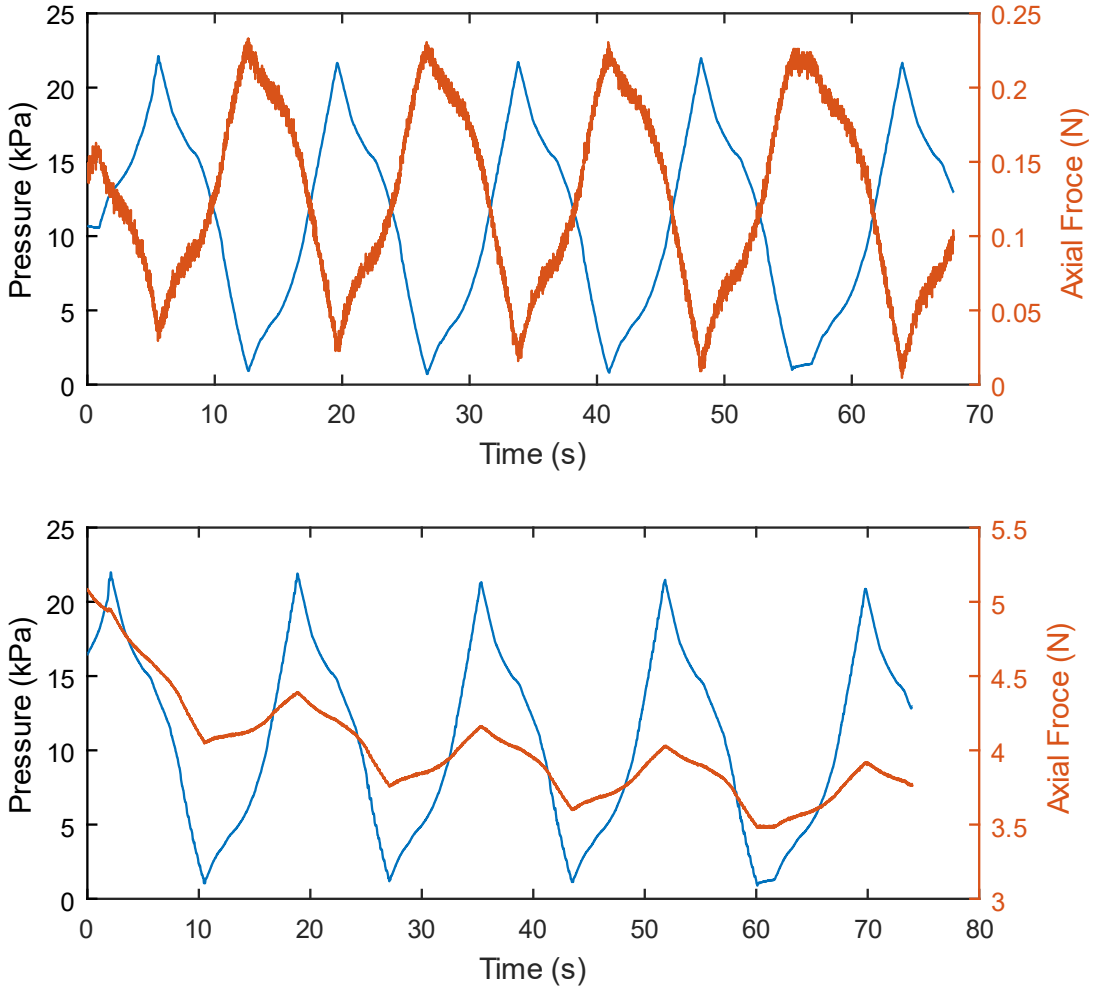

Figure 2.5. In vivo length identification graph sample. This figure shows two graphs comparing the axial forces and pressure values during pressurizing cycles, while the axial stretch is kept at a constant value. The top graph shows the sample's behavior when it is kept at a length less than the in vivo length. The bottom graph is depicting values when the artery is kept at a length greater than its in vivo length.

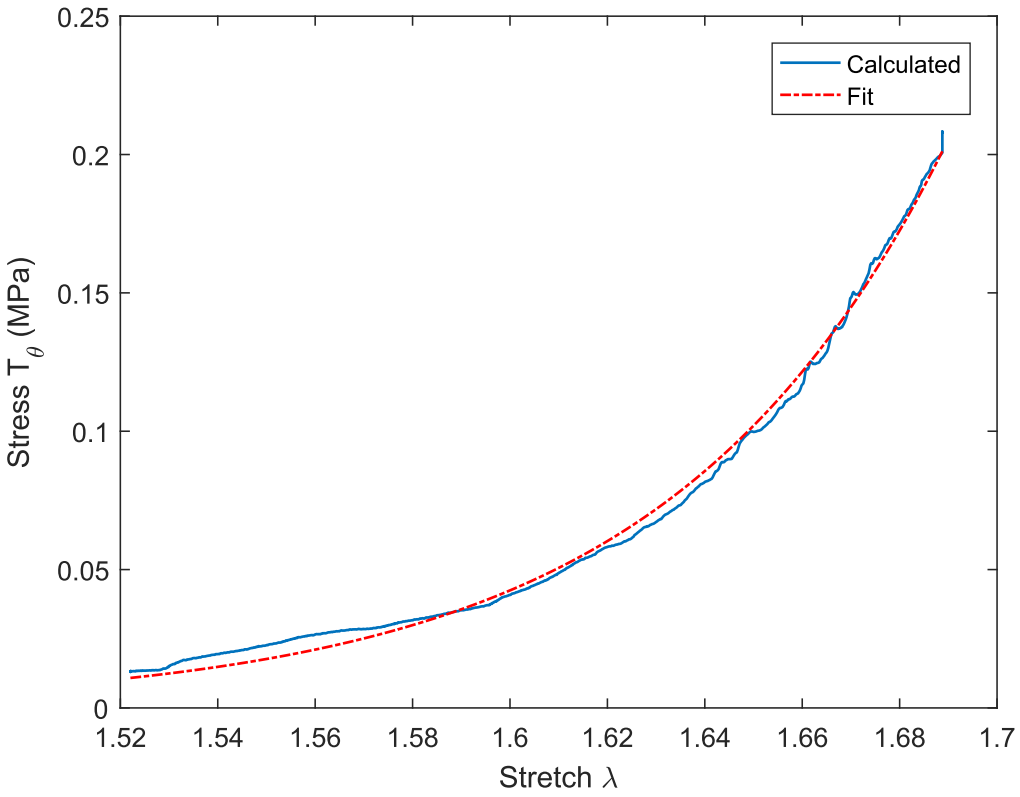

Figure 2.6. Sample stress-stretch curve fit. The smoothed circumferential stress-stretch curve is fit an exponential function using the least-squares method. This simplification was done to reduce the error in the calculations based on stress-stretch curves, for example, finding the in vivo stiffness.

CHAPTER 3

RESULTS

Results were evaluated both qualitatively and quantitatively to look for meaningful changes in sample behavior. Basic parameters were collected and calculated for the rest of the analysis (Table 3.1). Qualitative observation of the resulting stress-stretch curves for all sample groups demonstrated that some groups showed a relatively consistent shift between the control and NVS-treated samples. Circumferential stress-stretch curves for Groups 3 and 4, where the most consistent changes were observed, are presented in Figures 3.1 and 3.2 (circumferential stress-stretch curves of all groups are presented in Figure 3.4). In these figures, dashed lines identify the controls, and the solid lines identify the NVS-treated vessels, with pairs obtained from the same segment connected by arrows showing the direction of shift. While both groups showed a relatively predictable change with treatment, the direction of the shift was dependent on whether they did (Group 4; Figure 3.2) or did not (Group 3; Figure 3.1) receive a balloon expansion at the time of treatment. Stress-stretch curves from samples without balloon expansion during treatment tended to shift to the left, while for samples with balloon expansion, these curves tended to shift to the right. However, there were a small number of exceptions.

The same qualitative observations were carefully carried out for the axial stretch

direction, but there were no consistent changes in the axial properties of specimens in any of the groups (Figure 3.3), including Groups 3 and 4. It is notable that Groups 3 and 4 were not axially stretched during treatment. Similarly, no consistent patterns of change were observed for Groups 1 or 2 in either the circumferential or axial direction. This is true despite the fact that these groups were axially stretched to approximately in vivo length over the treatment period.

Quantitative analysis of these patterns revealed similar findings. Changes in circumferential in vivo stretch for Group 3 showed an average reduction in stretch (-0.112 ± 0.267; mean ± standard deviation) for treated samples compared to their respective controls. On the other hand, samples in Group 4 showed the opposite pattern, with increasing stretches compared to controls ($+0.140 \pm 0.206$). This can be seen clearly in the comparison box plots (Figure 3.5) as the median value lines for Groups 3 and 4 are offset in the negative and positive directions from zero, respectively. This difference between Groups 3 and 4 is about 0.25 stretch units. Comparison of the in vivo stiffness change between Group 3 (-0.0875 ± 0.7279) and Group 4 (-0.021 ± 0.272) shows that although their mean is closer to zero than the stretch values, the standard deviation for the stiffness is higher (Figure 3.6).

One-sample t-tests were performed for each group to test whether their properties deviated from the initial state. These tests revealed that neither of the groups' changes were statistically different from zero ($p > 0.05$).

ANOVA analyses were performed to identify whether the observed changes between the groups have a statistical significance. For the change of in vivo circumferential stretch values, using a Levene's test samples showed a homogeneous

variance. Consecutively, a simple one-way ANOVA test was conducted on these values among the four groups to evaluate whether there is a correlation between the groups. The resulting p value ($p=0.152$) was compared to the corrected threshold for significance (to confirm whether $p<0.0125$), adjusted using Bonferroni correction (dividing the significance threshold of 0.05 by the number of groups involved). The comparison showed no significance in the results.

For the change in the circumferential stiffness (Figure 3.6), as the variances were not homogenous, Welch ANOVA was conducted to consider the different variances. The results were insignificant between the groups. This implies that the arteries did not get stiffer in either the axial or circumferential direction at the in vivo configuration as a result of the treatment.

Since no ANOVA test resulted in a significant p-value(Table 3.4), no post hoc tests were needed to be performed.

Table 3.1 Average values measured and calculated from the entire sample population.

Initial outer diameter (mm)	**Initial inner diameter (mm)**	**Initial vessel wall area (mm^2)**	**In vivo circumferential stretch (mm/mm)**	**In vivo circumferential stiffness (MPa)**	**Balloon-induced circumferential stretch (mm/mm)**
3.861	2.063	8.38	1.651	1.90	2.009

Table 3.2 Change of in vivo circumferential stiffness and stretch values for different testing groups.

Testing Group	Change of in vivo circumferential stiffness		Change of in vivo circumferential stretch		Degrees of Freedom
	Mean	Standard Deviation	Mean	Standard Deviation	
Group 1	-1.253 e-1	0.627	-9.26 e-2	0.1561	5
Group 2	-2.81 e-2	0.578	6.65 e-5	0.249	6
Group 3	-8.75 e-2	0.728	-1.118 e-1	0.267	6
Group 4	-2.13 e-2	0.272	1.400 e-1	0.206	7

Table 3.3 One-sample t-test results for each group, including results for both change of in vivo circumferential stiffness values and change of in vivo circumferential stretch values.

Group:		**Group 1**	**Group 2**	**Group 3**	**Group 4**
Change of in vivo circumferential stiffness	**p-value (one-tailed)**	0.677	0.549	0.619	0.584
Change of in vivo circumferential stretch	**p-value (one-tailed)**	0.897	0.500	0.845	0.952

Table 3.4 Analysis of variables using ANOVA tests were performed and suggested insignificant p values. The p values were compared with the threshold 0.0125 based on Bonferroni correction.

	Levene test p-value	**ANOVA p-value**	**Welch ANOVA p-value**
Change of in vivo circumferential stiffness	0.0336	N/A	0.983
Change of in vivo circumferential stretch	0.563	0.152	N/A

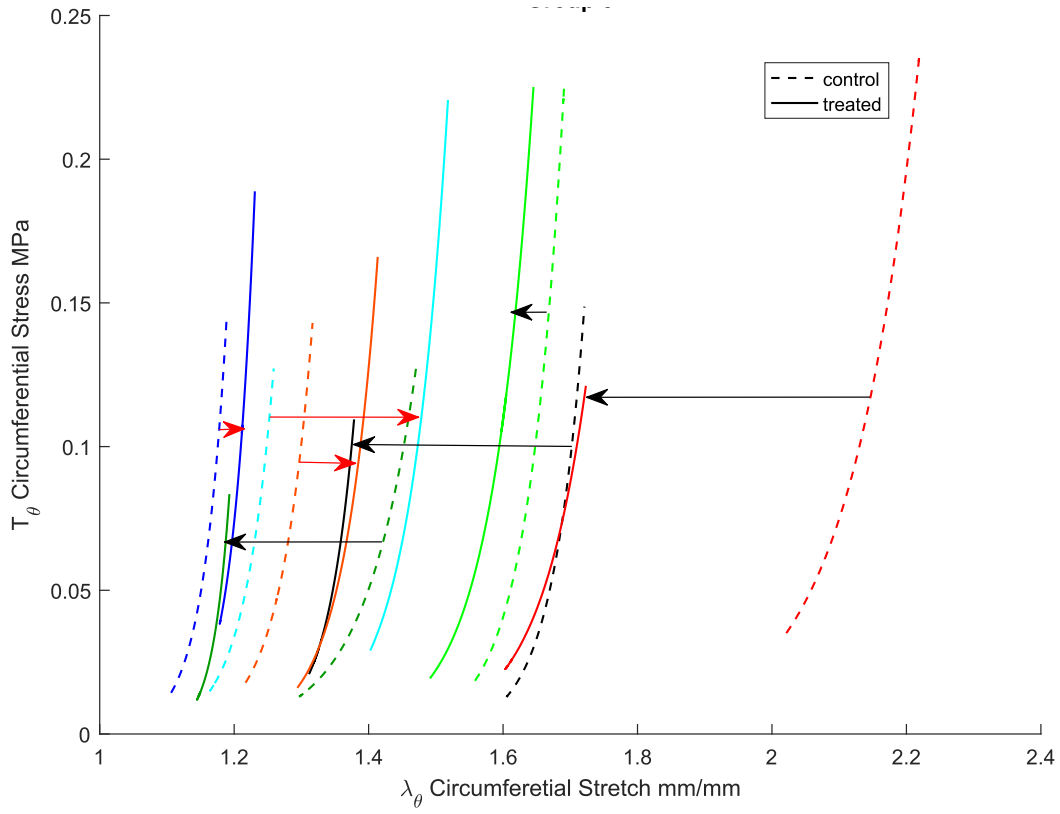

Figure 3.1. Stress-stretch curves for samples of Group 3 (not ballooned, no axial stretch). The shifts observed in the stress-stretch curves are indicated with the arrows connecting each control sample to its treated counterpart. The majority of the treated samples in this group showed a shift to lower stretch values (black arrows), but the behavior was not statistically significant (p=0.845).

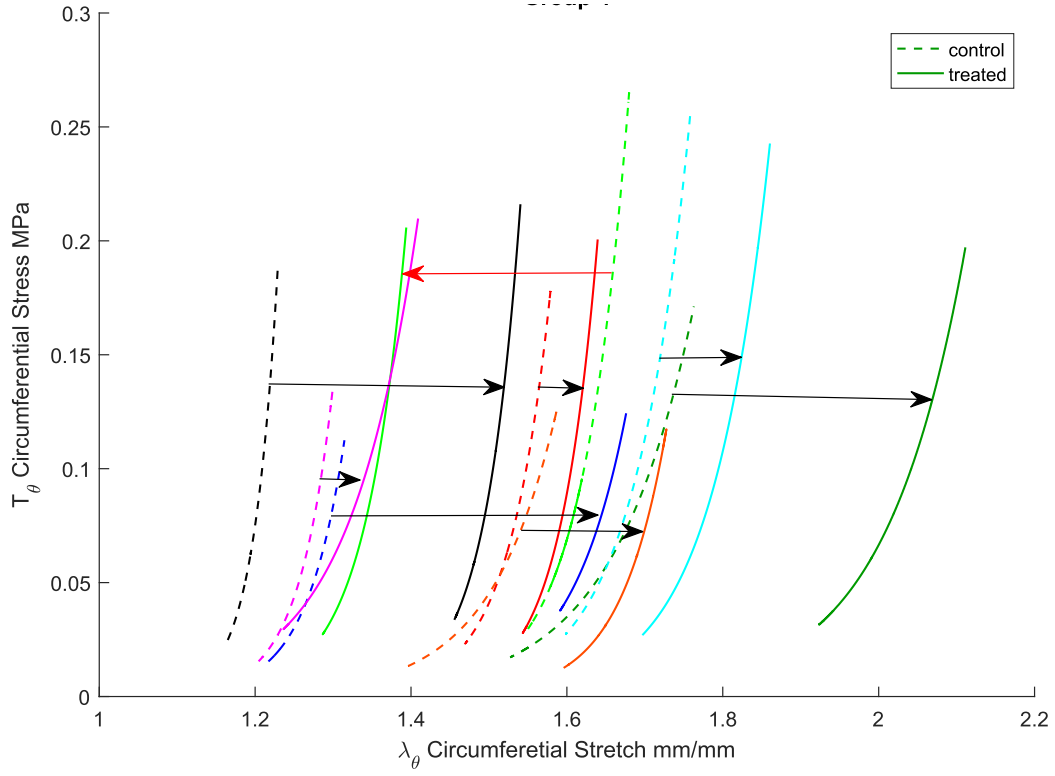

Figure 3.2. Stress-stretch curves for samples of Group 4 (ballooned, no axial stretch). The shifts observed in the stress-stretch curves are indicated with the arrows connecting each control sample to its treated counterpart. Most of the samples in this group showed a shift to higher stretch values (black arrows). This shift was statistically insignificant (p=0.952).

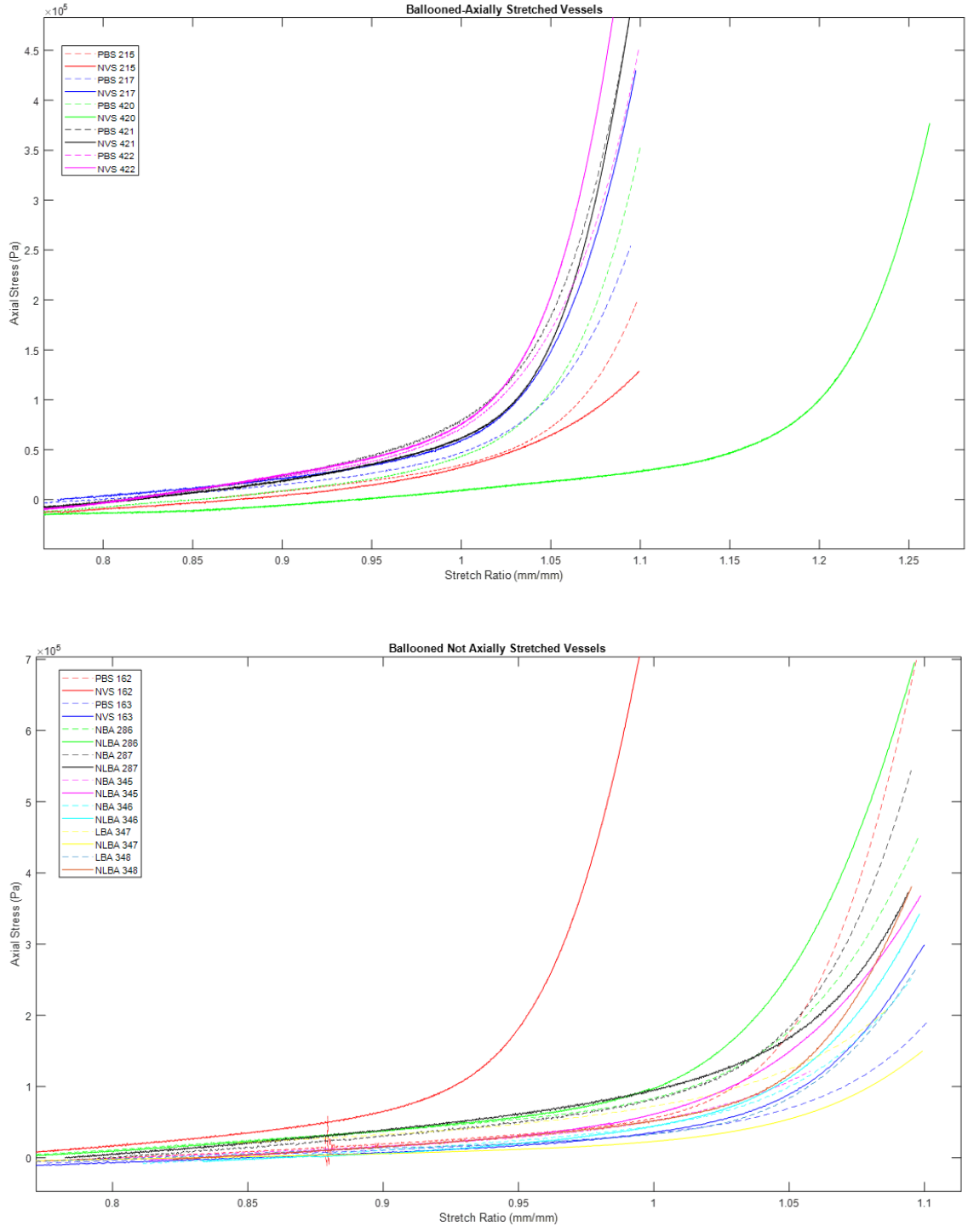

Figure 3.3. Axial stress-stretch curve sample from the ballooned and axially stretched group(top) and ballooned and not axially stretched group(bottom). The stretch values are normalized by the in vivo stretch in these figures. No correlations were found between treatments and changes in the samples' axial behavior.

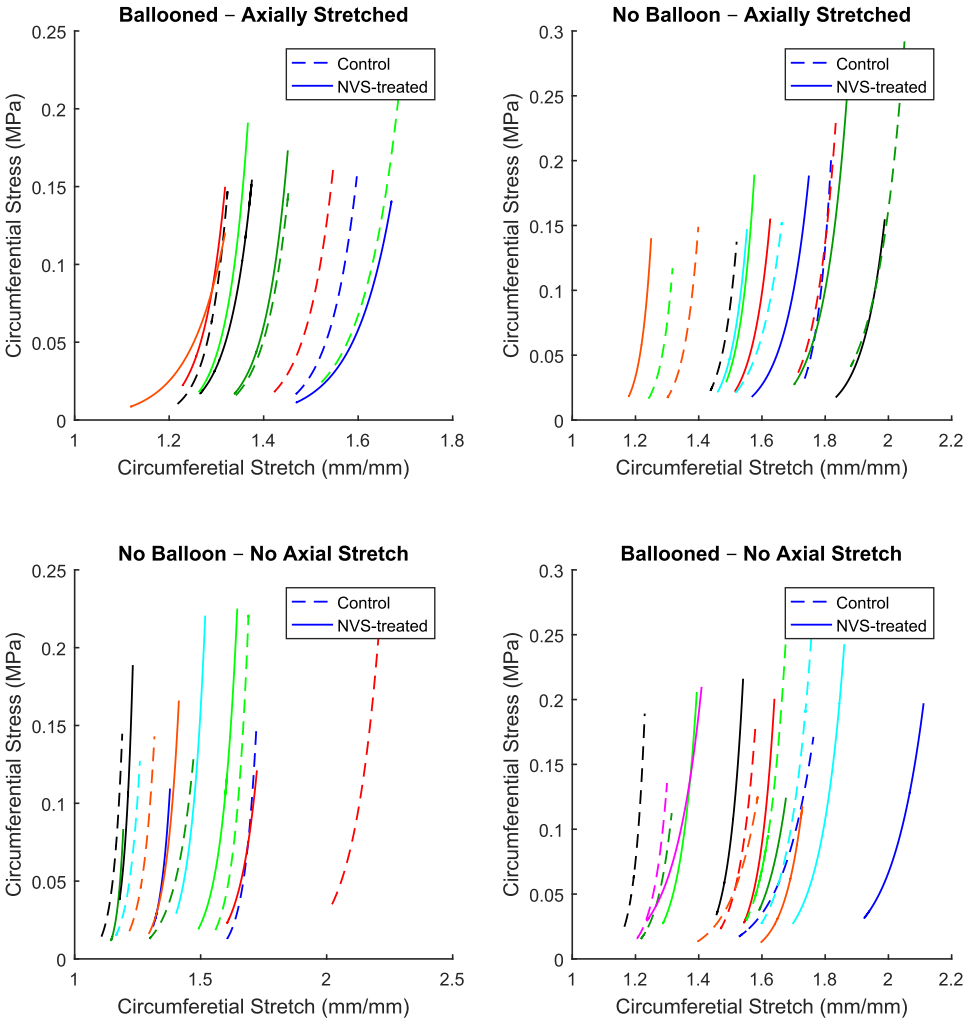

Figure 3.4. Circumferential stress-stretch response of treated and untreated vessels in all four groups.

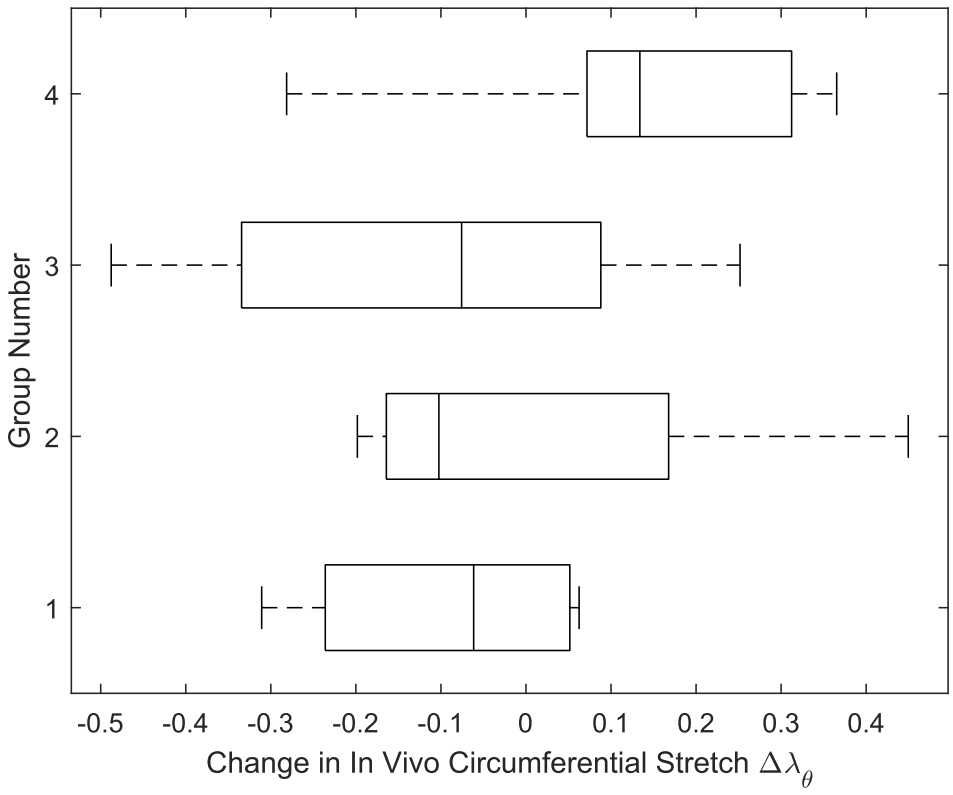

Figure 3.5. Comparison of circumferential in vivo stretch change in all four groups. The box plots represent the lowest and highest value observed, as well as first and third quartiles and the median.

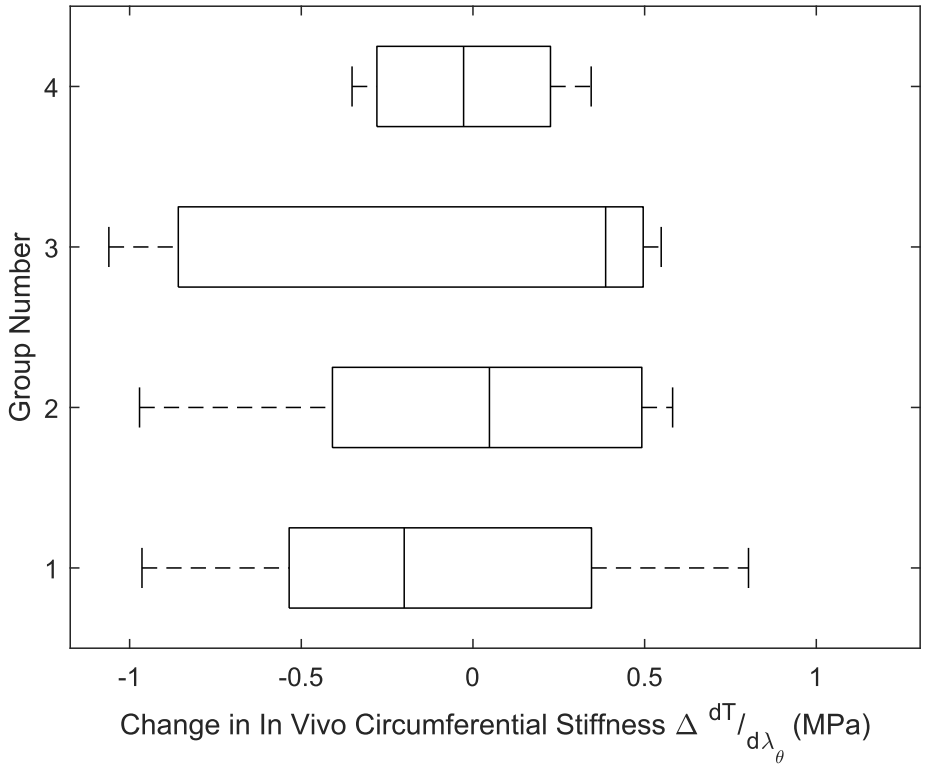

Figure 3.6. Comparison of circumferential in vivo stiffness change in all four groups

CHAPTER 4

DISCUSSION AND CONCLUSIONS

4.1 Study Objective Overview

The purpose of this study was to investigate the effects of NVS on the mechanical properties of arteries. NVS treatment is meant to be a replacement for stent placement in peripheral vascular disease treatment. It is intended to deliver the same functionality as stents by maintaining luminal patency while reducing the risks associated with stent placement in vessels that experience large deformations. Considering the aim of the study, we evaluated the influence of loading conditions at the time of NVS treatment on the behavior of porcine carotid arteries. The applied loading conditions were chosen based on the in vivo loadings that arteries experience during PTA surgery.

4.2 Findings of the Study

Among the different configurations under which the blood vessels were treated, circumferential loading of the artery at the time of treatment showed to have the most noticeable effect on the outcomes. The effectiveness of the treatment was measured in terms of change of in vivo circumferential stretch compared to the non-treated control groups. By comparing the changes, specifically for Group 3 and Group 4 (Figure 3.5), it was observed that depending on whether the samples were circumferentially loaded or

resting at the time of NVS activation, regardless of the axial stretches imposed on the sample, the circumferential in vivo stretch of the sample changed accordingly; i.e., it increased under stretch and decreased when treated at rest. Statistical analysis of variables, however, did not show this change to be statistically significant between the groups. This is while the circumferential stiffness of the samples did even show any visible change patterns in any of the groups (Figure 3.6). These results show that depending on loading at the time of treatment, NVS may be helpful to be used to change the working or physiological diameter of a blood vessel without altering its resistance to pressure-induced expansion. But to prove its functionality more testing and bigger sample population is needed.

It is notable that the influence of NVS treatment was only noticed in the circumferential response of the vessels. While the specifics of the cross-linking associated with NVS are still unknown, we can rely on knowledge of the microstructure of carotid arteries to help explain this observation, particularly if we assume that NVS influences collagen fiber cross-linking in some way. Microscopy examining the diffusion of the NVS compound shows that it typically did not diffuse beyond halfway through the vessel wall in these in vitro experiments (Figure 4.1). However, during some preliminary in vivo experiments done by our collaborators, it was observed that using the same treatment protocol, deeper diffusion of NVS was achieved. This could be due to other in vivo conditions that were not considered during in vitro treatment, for example, the sample being at body temperature or the presence of luminal pressure prior to treatment. Luminal diffusion during in vitro experiments was thus limited to influencing tissue constituents within the intima and media. Given that collagen fibers in the media of

carotid arteries are primarily oriented in the circumferential direction [11], it may not be surprising that the axial direction was unaffected. In addition, the direction of expansion in PTA balloons could be another reason why axial properties are not affected as they are expected to expand a vessel mostly circumferentially, so even in the absence of NVS, any softening or damage to the vessel would be expected to be primarily in the circumferential direction. That increases the probability of observing a pattern in changing properties in the circumferential direction.

The ability to manipulate the working diameter of a blood vessel without changing its stiffness could have a significant impact on the biomedical industry. The benefits of such tissue modification for intravascular intervention are apparent since the modification will treat the issue, which is often blood flow restriction, while the tissue continues to behave normally under mechanical loads of daily activities. This tissue property modification may also have an impact on a variety of applications for the treatment of different vascular disease conditions.

Similar to our work here, previous investigators showed that NVS could be used to minimize angioplasty-induced changes in vessel properties while retaining some of the desired luminal gains of the procedure [5]. While our findings are qualitatively similar to theirs, a quantitative comparison is difficult due to the use of different parameters to characterize vessel properties. Regardless, our results appear to confirm theirs and further reveal the importance of loading conditions at the time of treatment to effect the desired changes.

4.3 Other Aspects Explored

To check the possibility of other variables playing a significant role in the observed patterns, we ran a series of tests that isolated specific steps of the treatments. For example, we did some tests by only exposing the samples to the activation laser, or just the NVS compound without any activation laser exposure, or just performed the ballooning step. None of these tests showed a repeating and meaningful pattern that we could conclude that parameter played a significant role in the treatment, individually. Some of these test results are reported in Appendix B.

While the objective of this research was to evaluate changes in vessel mechanical properties with NVS treatment, we also performed some preliminary research into possible microstructural damage. Previous studies observed molecular level collagen damage in cerebral arterial tissues under overstretching using collagen hybridizing peptide (CHP) [12]. In the present study, we ran a series of preliminary staining and imaging experiments based on the protocol introduced in those studies. We stained treated and control samples to observe any differences between the samples' staining patterns among different groups. In our CHP study, both control and NVS-treated samples were overstretched circumferentially but not axially. Considering the fluorescent properties of NVS, wavelength overlapping of CHP and NVS signals was an issue for identifying and comparing the CHP staining patterns in initial studies (Figure 4.3). Therefore, we obtained a different version of CHP molecules tagged with markers having a different wavelength than the ones used in our reference research. Despite using this new CHP, no apparent difference between the NVS treated and control samples were observed. This finding was surprising since the carotid arteries were clearly overstretched; further study is needed and is ongoing in the Head Injury and Vessel

Biomechanics Laboratory to investigate the possibility that NVS might be binding to the damaged collagen fibers and, in a sense, acting as a healing agent to the overstretched collagen fibers involved in PTA. As previous studies have suggested, collagen and elastin cross-linking play an important role in the post-angioplasty healing of arteries[13]; this method could be an accelerated method to induce such cross-linking.

4.4 Limitations and Suggestions for Future Studies

One of the critical conditions used to simplify the calculations was assuming dimensions of the blood vessel wall stayed the same over sample length. We assumed they would be similar to a hollow tube and the wall dimensions to be equal to the average values calculated at the ends. This basically removes any local effects on the results and combines a possible range of results into one single value for the stress and one single value for the stretch across the sample at each timestep. In return, this approximation gives us the advantage of reducing the chances of capturing the end-effects and errors by averaging everything. However, if region-specific results are required in future studies, it is recommended that a different approach for dimension calculation be used across the sample length. Some suggestions for doing so would be using high-resolution MRI or intravascular ultrasound (IVUS) by placing the blood vessels in a contrasting medium and measuring dimensions over the entire length of the sample.

The main limitation of this study was not having enough samples to derive a conclusive statistical analysis of variables to evaluate the results. Due to the time-consuming nature of these experiments, after almost two years of experimenting, only the reported number of groups were reliable tests and that is simply not enough for

experiments of such nature to obtain statistical significance. To draw more accurate conclusions, as the variability of samples and testing groups makes it difficult to reach a statistically significant conclusion with few samples, more testing would be needed for the results to be reliable and identify effectiveness of the treatment.

To further explore the extent to which NVS is effective, several pathways can be defined for further experiments. The goal of these new experiments should be to minimize the chance of inconsistent behavior and incorrectly identified outliers. One pathway expected to lead to more reliable results would be to conduct both control and treated experiments using the same sample. This is achievable by evaluating a blood vessel's mechanical properties both before and after NVS treatment. The project sponsors did not initially propose this approach, but after our experiments, it was suggested and agreed upon by both our lab and the project sponsors, and the results are expected to be available soon.

Another approach to minimizing inconsistency in results would be to minimize the assumptions made during the testing and calculation of the results. For example, by observing the regional stress-stretch distribution on a sample, we might find a non-uniform distribution of change in properties due to NVS treatment. This non-uniform distribution could be caused by the varying microstructure of the extracellular matrix over the sample length. However, we do not expect the average values calculated by our methods to be substantially different from these non-uniform local stress-stretch values because we inspected the samples to have uniform and normal structures prior to selection for testing.

Another approach that could improve the correlation between NVS treatment and

changes in the properties of vasculature would be to investigate the concentration of NVS or, in other words, the number of NVS-bindings per unit volume within the sample. This would be an advantage to the prior assumption of binary NVS presence since the diffusion of NVS could be different for different samples (Figure 4.1), as they vary in microstructure and, hence, controlling only exposure time would not necessarily result in a fixed amount of NVS.

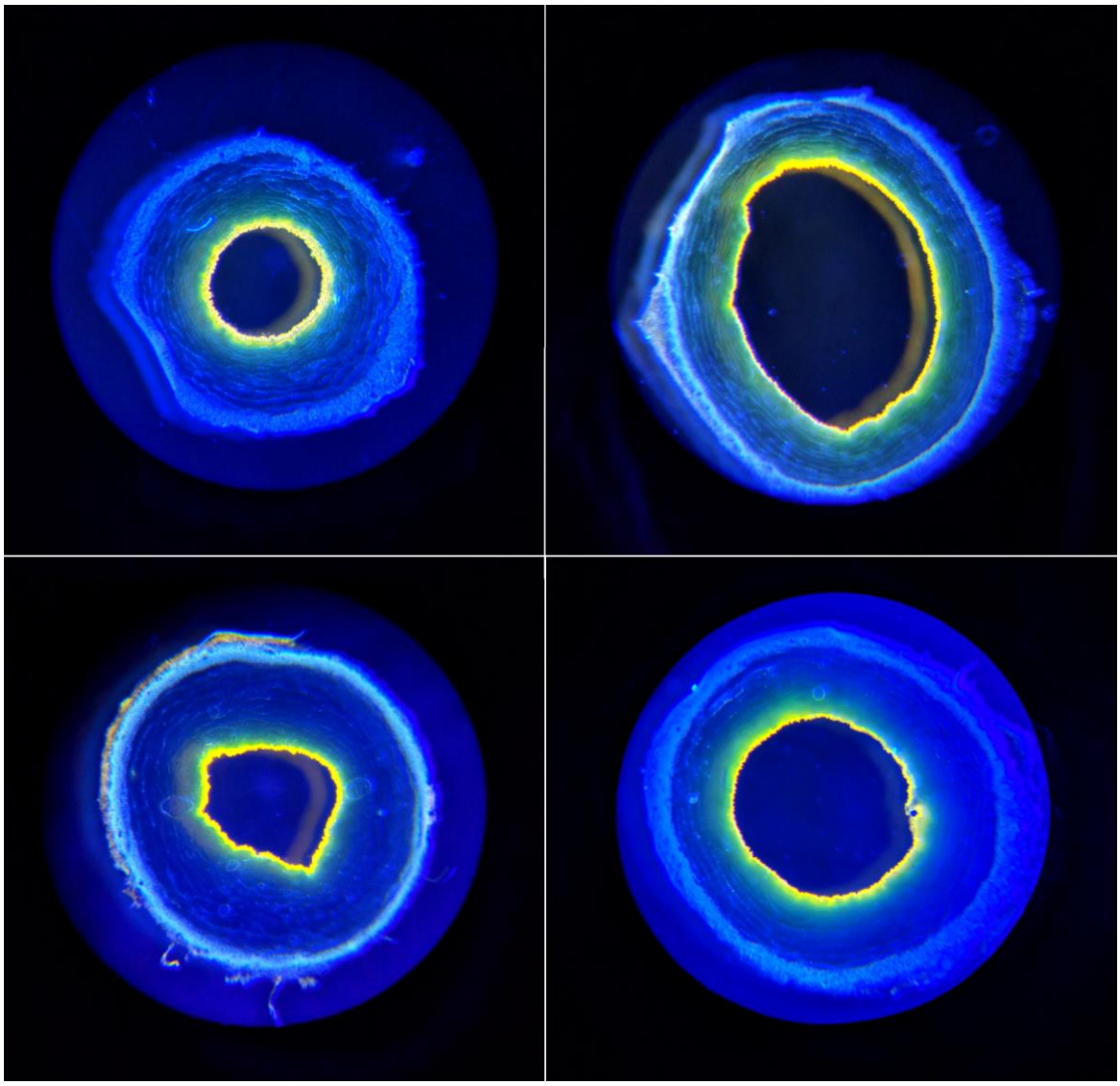

Figure 4.1. NVS-treated blood vessels cross-section. The bright yellow color is showing NVS presence. As seen, NVS yellow color covers the interlining then fades through the vessel wall. Bright yellow indicates the highest concentration of NVS, and as the yellow fades into the dark blue in the medial layer of the blood vessel wall, less NVS is present. Samples undergoing the same treatment protocol showed slightly different depth and regional patterns of NVS diffusion, as can be seen in Figure 4.2.

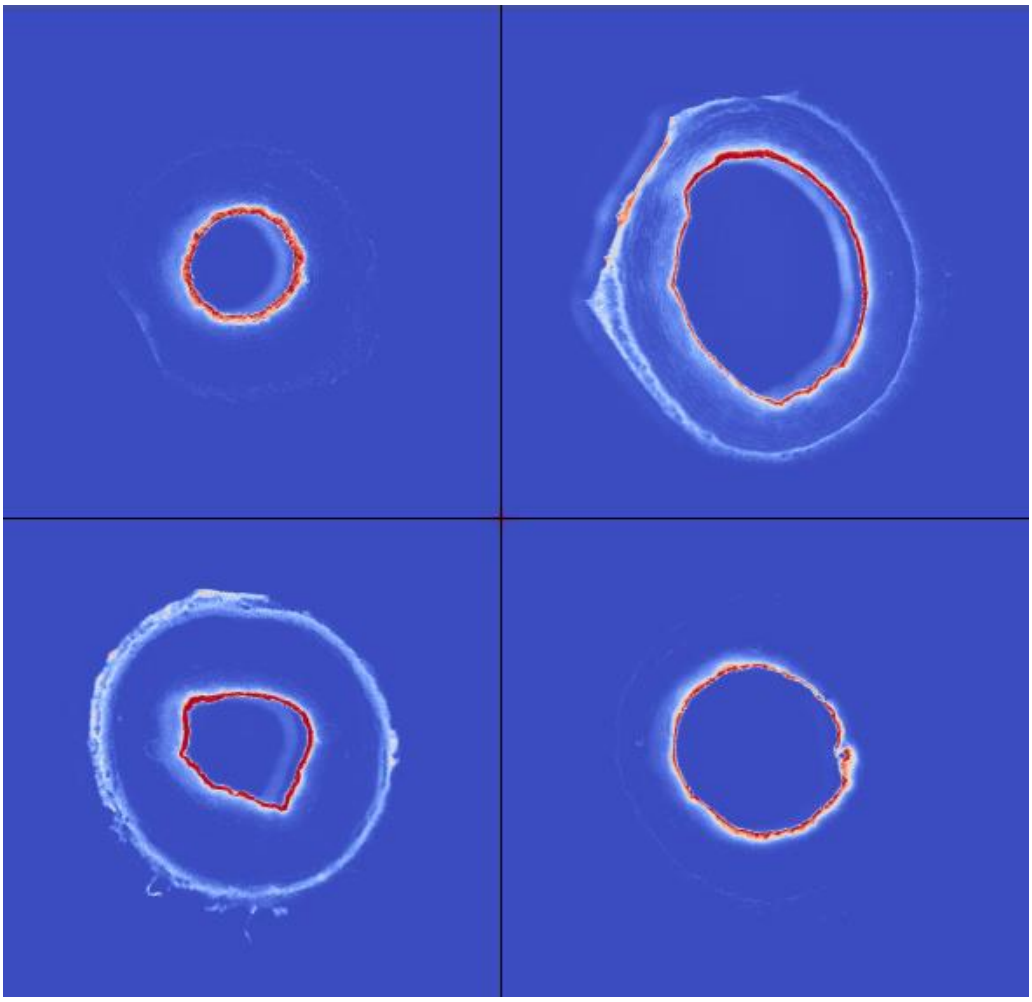

Figure 4.2. NVS diffusion map in Figure 4.1 samples. By extracting the yellow channel from Figure 4.1, the regions having the highest NVS concentrations are indicated in red on a blue background. Please note that the samples that have some red on the outer wall are expected to have been exposed to some NVS leakage in the petri dish.

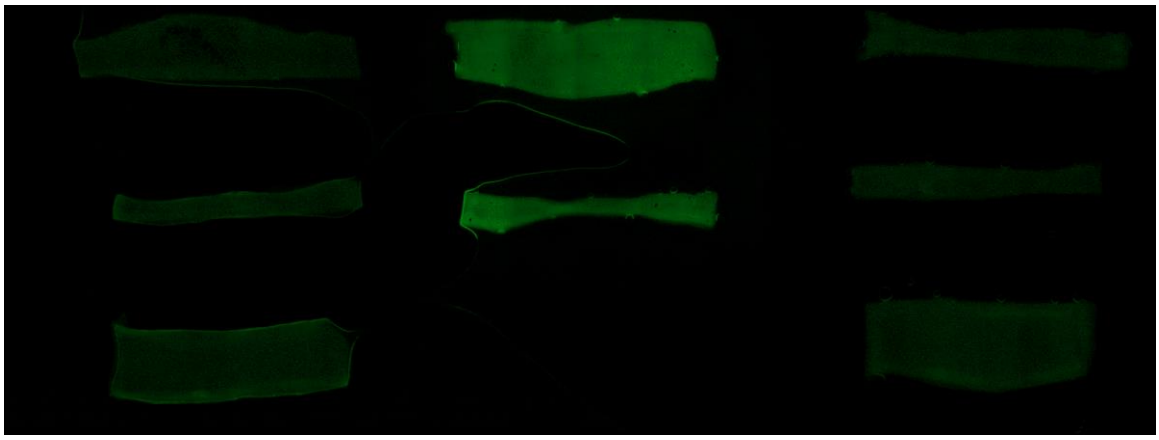

Figure 4.3. CHP-stained arteries microscopy image example. The CHP staining was done on three types of tissues for initial comparisons; Fresh arteries that underwent no testing (right), NVS-treated (middle), and control samples that were tested the same as NVS-treated samples (left). As it is clearly seen in this fluorescence microscopy image, the fluorescent illumination of the NVS sample is stronger than the CHP staining illumination. Therefore, the use of a different marker stain was necessary, but initial observation of that marker did not inform any decisions into the study..

APPENDIX A

MATLAB CODES

The code for cross-sectional area (CSA) measurement in MATLAB is as followed. Please note that the purpose of this code is to know the procedure to do the measurement and there might be functions needed that are not included in this script.

```
% Title: MeasureCSA.m
% Purpose: measure the cross-sectional area of vessels using a single
image of the cross-section

%%… initial preparation steps

% Draw outer perimeter
display('Using several clicks, define outer perimeter')
[BWo,xo,yo] = roipoly(I); close all; clc

% Draw inner perimeter
display('Using several clicks, define inner perimeter')
[BWi,xi,yi] = roipoly(I); close all; clc

% Calculate area
AreaO_pix = sum(sum(BWo));
AreaI_pix = sum(sum(BWi));
CSA_pix = abs(AreaO_pix-AreaI_pix);
CSA = CSA_pix*(mm_pix)^2;

% Calcualte outer diameter
n = length(xo);
perim_pix = 0;
for i = 1:n
    x1 = xo(i); y1 = yo(i);
    if i == n
        x2 = xo(1); y2 = yo(1);
    else
        x2 = xo(i+1); y2 = yo(i+1);
    end
    len = ((x2-x1)^2+(y2-y1)^2)^0.5;
    perim_pix = perim_pix + len;
end
perim_mm = perim_pix*mm_pix;
OD = perim_mm/pi;

% Calculate wall thickness from measured CSA and outer diameter
```

```
ID = (OD^2-(4/pi)*CSA)^0.5;
h = (OD-ID)/2;

%%… final representation steps
```

The code for stiffness calculation in MATLAB is as followed.

```
% Title: ModulusExtractor.m
% Purpose: calculates circ stretch and stiffness at inVivo P

%%… initial preparation steps

lamth=(di+od2)./(zDi+zod);
Tth=P./1000.*di./(od2-di);
lamth_iv=(di+od2)./(ivInnerDiam+ivOuterDiam);
Tth_iv=P./1000.*di./(od2-di);

fitFunc=fit(lamth,Tth,'exp1');

ivCircStretch=(ivInnerDiam+ivOuterDiam)./(zDi+zod);%calculates circ
stretch at inVivo P
ivCircStiffness=fitFunc.a*fitFunc.b*exp(fitFunc.b.*ivCircStretch);%calc
ulates circ stiffness at inVivo P
disp('E @IV circ stretch =');
ivCircStiffness
disp('IV Circ Stretch:');
ivCircStretch
```

APPENDIX B

EXTRA CONTROL GROUPS

A series of extra control tests were conducted to evaluate each step of the treatment's effects by isolating it individually and comparing the results to the qualitative effects we observed when performing the complete treatment.

Questions addressed include the following: Does shining the laser without NVS diffusion affect the vessels? Does diffusing the samples with NVS without any activation laser affect the tissue? And, do ballooned samples differ from the two former groups significantly? The following figures (B.1-B.3) show the results of these tests, in none of which we found a noticeable pattern.

We were also uncertain that there might be effects of calcium activation of the smooth muscle cells in results, as the samples were delivered to us in unknown PBS. Not considering this, for some samples, we did not change the saline. We made sure samples were submerged in calcium-free PBS after noticing this issue and compared those results with results from unknown saline. There was no difference in the outcome in terms of the resulting distributions (data not shown).

Another concern we addressed was ambient lighting effectively changing the amount of cross-linking and changing sample properties after being treated. We ran some tests with ambient light control, and the results were compared to the other samples. Ambient light control did not seem to affect the distribution of the results (data not shown).

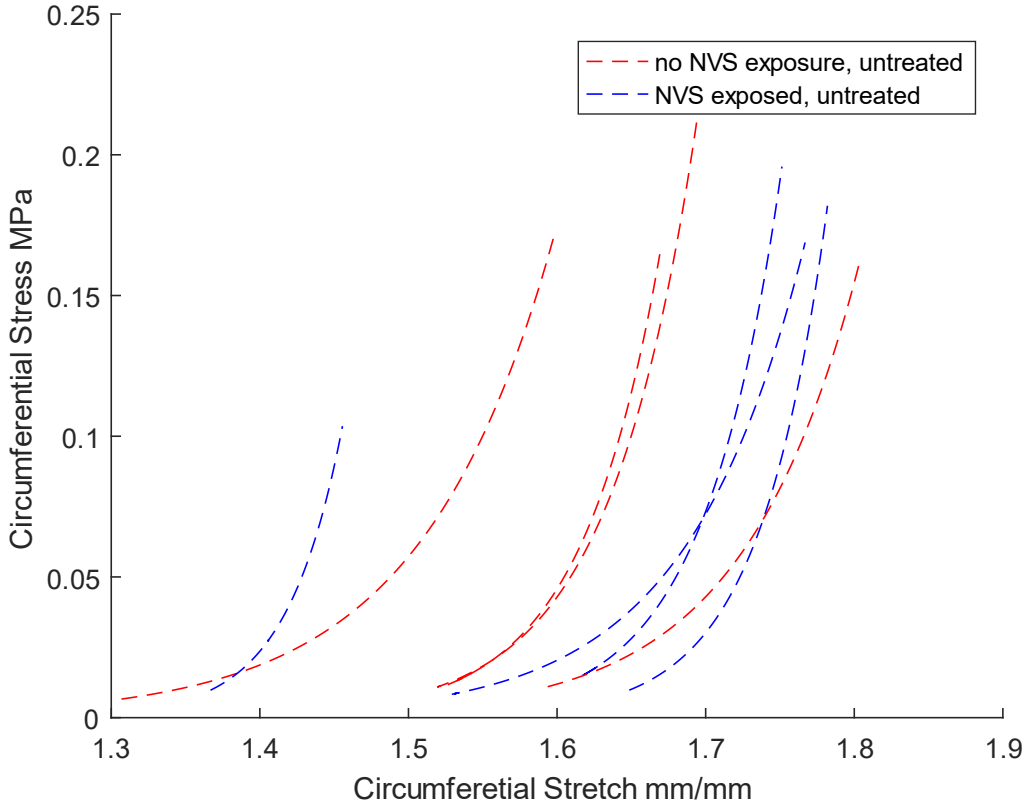

Figure B.1. The effect of non-activated NVS was evaluated. This was done by alternating NVS exposure while no laser activation was conducted, and only ballooning was done afterward. No trend in the resulting stress-stretch curves was observed. The term "untreated" in the figure's legends means that the complete NVS treatment was not conducted on samples as they were not exposed to the activation laser.

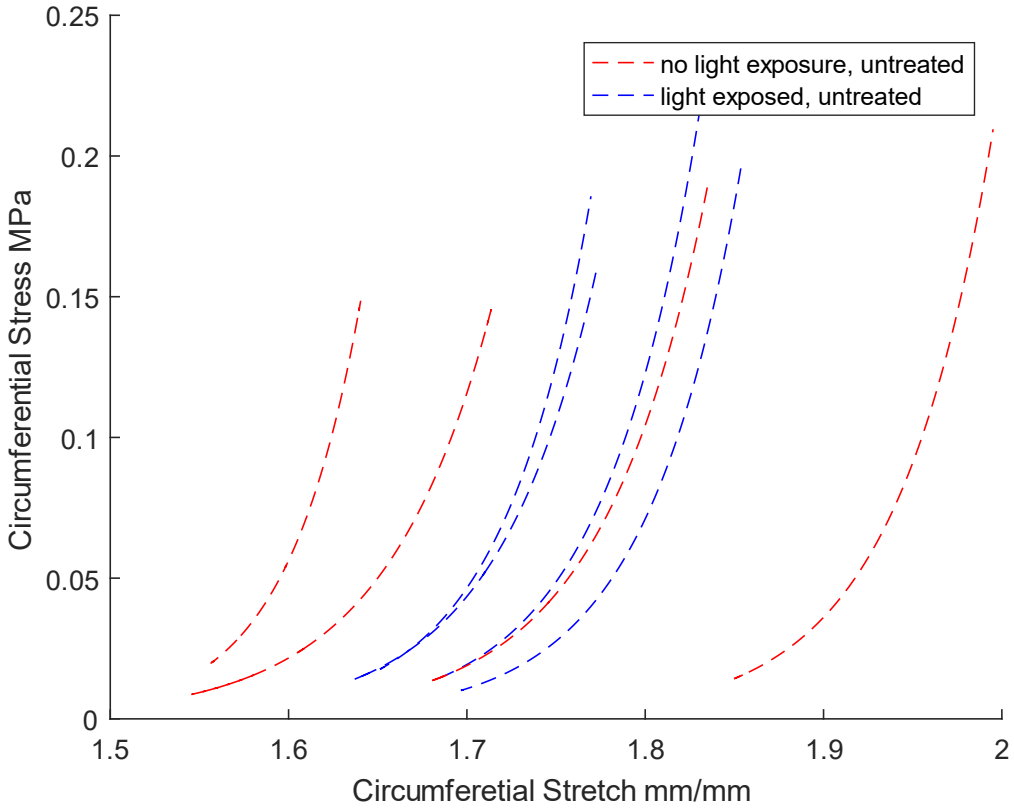

Figure B.2. The effect of activation laser during the treatment was evaluated. Alternating laser exposure was conducted in the absence of NVS, and the samples afterward were ballooned during laser exposure or while the laser was off in the other samples. No trend in the resulting stress-stretch curves was observed. The term “untreated” in the legend means that the complete NVS treatment was not conducted on samples as they were not exposed to NVS.

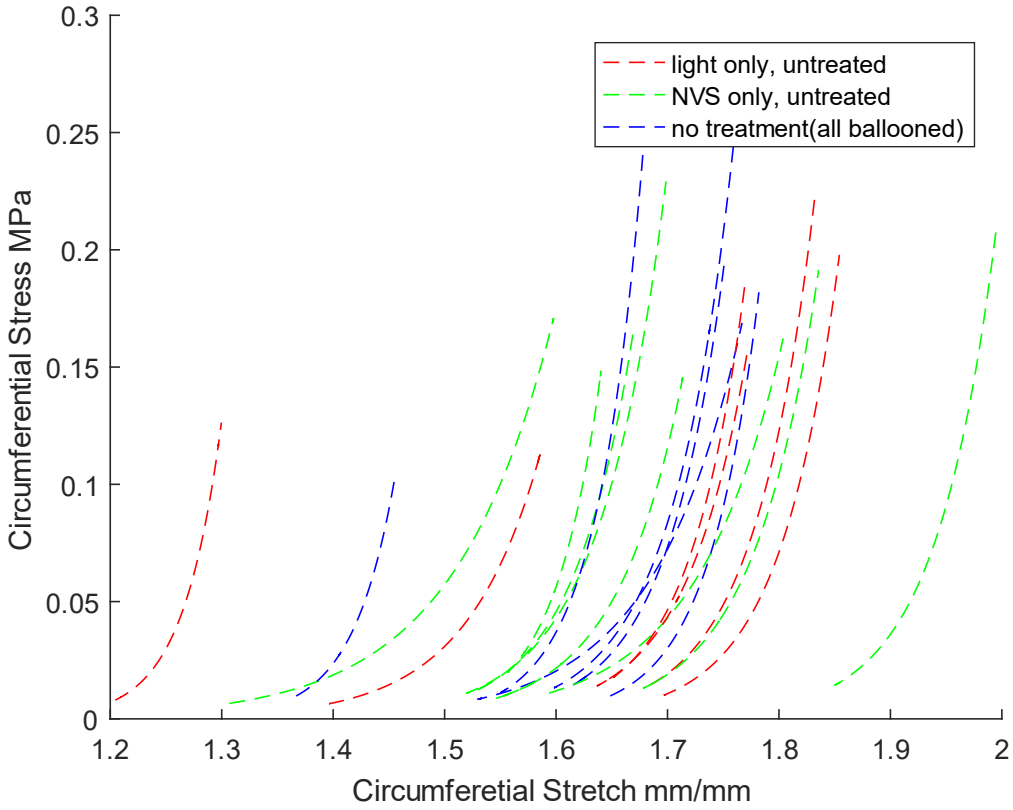

Figure B.3. Untreated samples were compared to ballooned samples population to observe the results for noticeable clustering of groups. No patterns or significant distribution was observed. The term “untreated” in the legend means that the complete NVS treatment was not conducted on samples as they were not exposed to either NVS or the activation laser.

REFERENCES

[1] Mozaffarian, D., Benjamin, E. J., Go, A. S., Arnett, D. K., Blaha, M. J., Cushman, M., Das, S. R., de Ferranti, S., Després, J.-P., Fullerton, H. J., Howard, V. J., Huffman, M. D., Isasi, C. R., Jiménez, M. C., Judd, S. E., Kissela, B. M., Lichtman, J. H., Lisabeth, L. D., Liu, S., Mackey, R. H., Magid, D. J., McGuire, D. K., Mohler, E. R., Moy, C. S., Muntner, P., Mussolino, M. E., Nasir, K., Neumar, R. W., Nichol, G., Palaniappan, L., Pandey, D. K., Reeves, M. J., Rodriguez, C. J., Rosamond, W., Sorlie, P. D., Stein, J., Towfighi, A., Turan, T. N., Virani, S. S., Woo, D., Yeh, R. W., and Turner, M. B., 2015, *Heart Disease and Stroke Statistics—2016 Update*.

[2] Lloyd-jones, D. M., Benjamin, E. J., Jarett, D., Borden, W. B., Bravata, D. M., Dai, S., Earl, S., Fox, C. S., Fullerton, H. J., Hailpern, S. M., Heit, J. a, Howard, V. J., Kissela, B. M., Kittner, S. J., Lackland, D. T., Lichtman, J. H., Lisabeth, L. D., Diane, M., Marcus, G. M., Marelli, A., David, B., Moy, C. S., Mozaffarian, D., Soliman, E. Z., Sorlie, P. D., and Sotoodehnia, N., 2012, "HHS Public Access," Circulation, **125**(1).

[3] Humphrey, J. D., 2002, *Cardiovascular Solid Mechanics*, Springer New York, New York, NY.

[4] Vossen, R. J., Vahl, A. C., Leijdekkers, V. J., Montauban van Swijndregt, A. D., and Balm, R., 2018, "Long-Term Clinical Outcomes of Percutaneous Transluminal Angioplasty with Optional Stenting in Patients with Superficial Femoral Artery Disease: A Retrospective, Observational Analysis," Eur. J. Vasc. Endovasc. Surg., pp. 1–9.

[5] Munger, K. A., Downey, T. M., Haberer, B., Pohlson, K., Marshall, L. L., and Utecht, R. E., 2016, "A Novel Photochemical Cross-Linking Technology to Improve Luminal Gain, Vessel Compliance, and Buckling Post-Angioplasty in Porcine Arteries," J. Biomed. Mater. Res. - Part B Appl. Biomater., **104**(2), pp. 375–384.

[6] Humphrey, J. D., 1995, "Mechanics of the Arterial Wall: Review and Directions," Crit. Rev. Biomed. Eng., **23**(1–2), pp. 1–162.

[7] Prim, D. A., Mohamed, M. A., Lane, B. A., Poblete, K., Wierzbicki, M. A., Lessner, S. M., Shazly, T., and Eberth, J. F., 2018, "Comparative Mechanics of Diverse Mammalian Carotid Arteries," PLoS One.

[8] Roubin, G., Mb, P., Douglas, J., King, S., Lin, S., Hutchison, N., Thomas, R., and Gruentzig, A., 1988, "Influence of Balloon Size on Initial Success, Acute Complications, and Restenosis After Percutaneous Transluminal Coronary Angioplasty: A Prospective Randomized Study," Circulation, **78**(3), pp. 557–565.

[9] Monson, K. L., Barbaro, N. M., and Manley, G. T., 2008, "Biaxial Response of Passive Human Cerebral Arteries," Ann. Biomed. Eng., **36**(12), pp. 2028–2041.

[10] Van Loon, P., 1977, "Length-Force and Volume-Pressure Relationships of Arteries.," Biorheology, **14**(4), pp. 181–201.

[11] Sáez, P., García, A., Peña, E., Gasser, T. C., and Martínez, M. A., 2016, "Microstructural Quantification of Collagen Fiber Orientations and Its Integration in Constitutive Modeling of the Porcine Carotid Artery," Acta Biomater., **33**, pp. 183–193.

[12] Marino, M., Converse, M. I., Monson, K. L., and Wriggers, P., 2019, "Molecular-Level Collagen Damage Explains Softening and Failure of Arterial Tissues: A Quantitative Interpretation of CHP Data with a Novel Elasto-Damage Model," J. Mech. Behav. Biomed. Mater., **97**, pp. 254–271.

[13] Brasselet, C., Durand, E., Addad, F., Al Haj Zen, A., Smeets, M. B., Laurent-Maquin, D., Bouthors, S., Bellon, G., De Kleijn, D., Godeau, G., Garnotel, R., Gogly, B., and Lafont, A., 2005, "Collagen and Elastin Cross-Linking: A Mechanism of Constrictive Remodeling after Arterial Injury," Am. J. Physiol. - Hear. Circ. Physiol., **289**(5 58-5), pp. 2228–2233.